Hydrogen Embrittlement of Automotive Advanced High-Strength Steels

GIANFRANCO LOVICU, MAURO BOTTAZZI, FABIO D'AIUTO, MASSIMO DE SANCTIS, ANTONELLA DIMATTEO, CIRO SANTUS, and RENZO VALENTINI

Advanced high-strength steels (AHSS) have a better combination between strength and ductility than conventional HSS, and higher crash resistances are obtained in concomitance with weight reduction of car structural components. These steels have been developed in the last few decades, and their use is rapidly increasing. Notwithstanding, some of their important features have to be still understood and studied in order to completely characterize their service behavior. In particular, the high mechanical resistance of AHSS makes hydrogen-related problems a great concern for this steel grade. This article investigates the hydrogen embrittlement (HE) of four AHSS steels. The behavior of one transformation induced plasticity (TRIP), two martensitic with different strength levels, and one hot-stamping steels has been studied using slow strain rate tensile (SSRT) tests on electrochemically hydrogenated notched samples. The embrittlement susceptibility of these AHSS steels has been correlated mainly to their strength level and to their microstructural features. Finally, the hydrogen critical concentrations for HE, established by SSRT tests, have been compared to hydrogen contents absorbed during the painting process of a body in white (BIW) structure, experimentally determined during a real cycle in an industrial plant.

DOI: 10.1007/s11661-012-1280-8

I. INTRODUCTION

IN the last few decades, the development of new classes of high-strength steels allowed for increasing both resistance and toughness properties in respect to conventional high-strength autobody steels. The transformation-hardened steels (the so-called advanced high-strength steels) along with high-manganese austenitic steels are examples of new recently developed classes.[1–4]

In conventional steels, more traditional hardening methods are used, such as solid solution, grain refinement, or precipitation, whereas in advanced high-strength steels (AHSS), less conventional ones, based on phase transformations, are applied. These methods allow for obtaining complex microstructures, where mechanical properties of transformed phases are, to some extent, merged. The main classes are dual phase (DP), transformation induced plasticity (TRIP), martensitic, complex phase steels, and others. They differ in terms of type and volume fraction of microstructural constituents.

GIANFRANCO LOVICU, Research Assistant, MASSIMO DE SANCTIS and RENZO VALENTINI, Associate Professors, and ANTONELLA DIMATTEO, Young Researcher, are with the Dipartimento di Ingegneria Chimica, Chimica Industriale e Scienza dei Materiali, Università di Pisa, 56126 Pisa, Italy. Contact e-mail: g.lovicu@ing.unipi.it MAURO BOTTAZZI and FABIO D'AIUTO, Sheets Specialists, are with the Centro Ricerche Fiat Scpa, 10043 Orbassano, To, Italy. CIRO SANTUS, Assistant Professor, is with the Dipartimento di Ingegneria Meccanica, Nucleare e della Produzione, Università di Pisa, 56126 Pisa, Italy.

Manuscript submitted January 28, 2011.
Article published online June 30, 2012

DP steels have a ferrite-martensite mixed microstructure[5] with a martensite volume fraction ranging from 20 to more than 75 pct in respect to the steel grade. The typical tensile strengths of DP steels are between 450 and 1100 MPa, and elongation is between 10 and 25 pct. The microstructure of TRIP steels consists of a ferritic matrix with dispersed islands of hard phase (bainite and/or martensite) and retained austenite.[5] During straining, the metastable austenitic phase transforms into martensite (TRIP effect), increasing both strength and ductility. Between steels belonging to AHSS, the martensitic steels have the highest strength levels. Two main groups could be highlighted, the cold-rolled martensitic steels for cold forming and the boron containing steels optimized for hot stamping. The typical tensile strength of martensitic steels can lie between 1000 and 1500 MPa. Despite their limited elongation and the high springback effect related to their high grades, cold-rolled steels have great potential thanks to their lower cost with respect to hot-stamping components of similar strength. On the contrary, the hot-stamping process allows for obtaining high-strength components with low residual stresses and a more homogeneous microstructure, but with higher costs.

Generally, by increasing the mechanical resistance of steels, also their hydrogen embrittlement susceptibility increases.[6–8] This general behavior is observed in steels belonging to the same class,[8] although some researchers stress the role of all the parameters that influence the hydrogen embrittlement susceptibility, such as microstructures, trapping state, deformation state, and strength.[9]

Hydrogen degradation could represent one of the main limitations to the use of advanced high-strength steels. In steel, hydrogen can derive from the production

process, product assembling, and finishing, or from service environment exposure. If the hydrogen content reaches a critical value inside the steel, it can induce a strong reduction of mechanical properties, particularly strength and ductility. In the case of conventional quench and tempered steels with a ultimate tensile strength (UTS) of about 1500 MPa, the critical value to induce hydrogen embrittlement can be much less than 1 wppm (see, for example, Reference 8). Since the largest parts of car body components are produced by cold-forming techniques that can induce high residual stresses, the effect of very little quantities of hydrogen can be catastrophic.

Although some experimental studies have been carried out on hydrogen embrittlement of AHSS,[10–14] much work is still needed. In particular, the hydrogen effect on multiphase steels should be better related to the peculiar microstructural features of steels. Above all, when an austenitic phase is also present, such as for TRIP steels, the effect of huge differences on transport and solubility properties of hydrogen within the austenite and the ferritic/martensitic matrix, as well the austenite tendency to transform to martensite during straining and/or during hydrogen charging, are all aspects of the problem that needs to be thoroughly investigated.

One main experimental technique used to analyze the hydrogen effect on mechanical properties of steels is the slow strain rate tensile (SSRT) test,[15] *i.e.*, a tensile test performed at a slow strain rate in order to enhance the embrittlement effect of hydrogen. The hydrogen embrittlement mechanism is governed by local hydrogen transport within the steels. The high-stressed areas (with a nonzero hydrostatic component) in the sample are subject (1) to a lattice distortion that can increase the local hydrogen solubility and thus (2) to generate a chemical potential gradient that can act as a driving force for the hydrogen diffusion. Thus, areas with higher residual stresses not only are subjected to a higher stress level but also are richer in hydrogen, dramatically increasing the failure susceptibility.

This article analyzes the hydrogen embrittlement behavior of four different AHSS by means of SSRT tests on electrochemically charged notched tensile samples. The obtained results, along with the fractographic studies of post-tensile samples, have been deeply investigated in terms of their microstructural and mechanical features. Finally, in order to compare the critical hydrogen concentrations determined by SSRT tests with the quantity of hydrogen absorbed in real conditions, particular attention has been put on the pretreatment of the painting process. As a matter of fact, phosphatizing and electrodeposition paint (EDP) processes could be responsible for some hydrogen absorption.[16] The hydrogen concentration absorbed from different tested steels has been measured using the barnacle electrode method after exposition of steel specimens to a real industrial process.

II. MATERIALS AND EXPERIMENTAL METHODS

A. *Materials*

Four different commercial AHSS have been selected in order to investigate their hydrogen embrittlement susceptibility. In particular, one hot-stamping, two martensitic, and one TRIP steels have been analyzed. All steels have been received in their commercial coating conditions. Hot-stamping steel has been received in quenched condition by using the same temperature and cooling rate as for the real industrial hot-stamping process.

Table I shows the chemical compositions along with the thickness and the coating characteristics of each studied steel.

In order to analyze their microstructures, each steel has been polished and then etched by employing appropriate reagents depending on the expected microstructures. Nital reagent has been used for hot-stamping and martensitic steels, while Le Pera etchant has been used to highlight the complex microstructure of TRIP 800 steel.

B. *Mechanical Tests*

Preliminary mechanical tests have been performed on as-received smooth tensile samples using a MTS 100 kN tensile machine (MTS Systems Corporation, Eden Prairie, MN), in order to measure the mechanical properties of as-received steels.

C. *SSRT*

Notched tensile samples, with the geometry and dimensions shown in Figure 1, have been used to carry out SSRT tests. The presence of a notch allows for obtaining a hydrostatic stress state in its proximity, thus, increasing the embrittling effect of hydrogen. Before hydrogenation, the sample surface had been prepared by removing the coating layer using SiC paper up to 600 grit.

Different electrochemical conditions have been used in order to obtain hydrogen contents ranging in a wide interval able to include the embrittlement of materials.

Table I. Thickness, Coating Type, and Chemical Composition of Tested Steels

			Chemical Composition						
Steel	Thickness (mm)	Coating Type	C (Pct)	Mn (Pct)	Si (Pct)	Cr (Pct)	Ti (Pct)	Al (Pct)	B (wppm)
HS 1500	1.80	Al-Si	0.22	1.25	0.25	0.22	0.04	0.04	>20
M 1400	1.25	electrogalv	0.18	1.51	0.35	0.21	0.04	0.05	>20
M 1200	2.00	electrogalv	0.12	1.70	0.21	0.03	0.03	0.04	>20
TRIP 800	1.12	galv	0.19	2.12	0.63	0.03	0.01	1.02	—

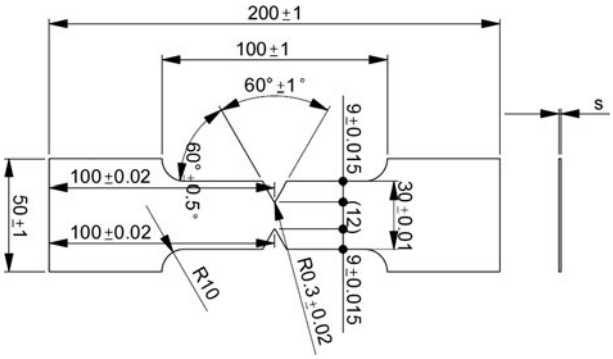

Fig. 1—Specimen geometry and dimensions for SSRT tests. The thickness *s* depends on the steel strip thickness.

Aqueous solutions containing NaOH (0.1 M), H_2SO_4 (0.1 N and 1 N) have been used, with the addition of different recombination poisons (As_2O_3, $NaAsO_2$). The cathodic current densities typically ranged from 1 to 50 mA/cm^2. Electrochemical charging time has been chosen with respect to the saturation time of each steel, depending on specimen thickness and hydrogen diffusion coefficient,[17] the latter measured by a Devanathan-Stackurski electrochemical permeation experiment.[18]

Coupons of the same steel have been hydrogenated contemporary to the tensile samples to have witness specimens in order to measure the absorbed hydrogen content before tensile tests. Hydrogen concentration has been measured using a LECO DH603 hydrogen determinator (LECO Corporation, St. Joseph, MI), based on the hot extraction method. SSRT tests have been performed following the ASTM G129 00 standard test method,[19] using a strain rate of about 4×10^{-5} s^{-1}.

After SSRT tests, one half of each fractured sample has been used for fractographic analysis, while the other half has been used to measure the post-tensile hydrogen concentration by using the LECO DH603.

D. *Hydrogen Absorbed During Painting Process*

Hydrogen uptake in autobody components may result from assembling and/or finishing processes. Because of the steel sheet thinness, no residual hydrogen is expected from the steel production process. Therefore, in this context, the painting process could represent its main source, as a consequence of the cathodic reactions in water solution that takes place in phoshatizing and electrophoresis stages.[16] During these reactions, atomic hydrogen can form on the steel surface. The main part of the hydrogen generated on steel surface recombines to form gaseous hydrogen, but some hydrogen can be absorbed and diffuse into the steel.

Some samples of the tested steels have been prepared and connected in a commercial body in white (BIW) structure in order to test the real cycle conditions. Tests have been performed in an industrial plant, during an usual production cycle. The main pretreatment process parameters are summarized in Table II. Three steps of the coating process have been analyzed: phosphatizing, EDP, and the final curing stages. After each step, three coupons of each steel have been extracted and stored in dry ice or liquid nitrogen until its hydrogen content has been measured in the laboratory.

Table II. Main Pretreatment Painting Process Parameters Registered During the Cycles Used for the Hydrogen Absorption Analysis

Phosphatizing	T = 323 K (50 °C)	pH = 4.7
Primer electrodeposition	V = 220 ÷ 310 V	pH = 6
EDP curing	T = 170 ÷ 190 °C	

For each sample, two different conditions of coating layer have been analyzed: the undamaged state and the case of scratches presence in the protective layer. The latter condition was chosen in order to simulate the effect of galvanic coupling between the protective layer and the underlying metal.

The measurement of superficial absorbed hydrogen has been done by the barnacle electrode method,[20] following the ASTM F1113 standard testing method.[21] The registered current output had been preliminary correlated to the hydrogen content using uniformly charged samples, whose hydrogen concentration had been measured using the hot extraction method (using a LECO DH603).

E. *Fractographic Analysis*

The post-tensile fractographic analysis has been performed using a JEOL 5600LV Scanning Electron Microscope (SEM) (JEOL Ltd., Tokyo, Japan), interfaced with an energy-dispersive X-ray spectrometer. The aim of these observations has been to highlight the correlation between the hydrogen concentration and the fracture modalities of each analyzed steel.

III. RESULTS

A. *Microstructural Investigation*

Figure 2 shows the optical micrographs of tested steels. Hot-stamping and martensitic steels have a martensitic microstructure. TRIP 800 steel shows a mixed microstructure composed of ferrite, bainite/martensite, and retained austenite, as expected. The Le Pera reagent, used for TRIP steel, allows for highlighting different phases with different colors. In particular, in Figure 2(c), ferrite appears light brown, bainite appears dark brown, and martensite and austenite appear white.

B. *Mechanical Properties*

Main mechanical properties, measured by tensile tests on smooth samples, are summarized in Table III. The measured mechanical properties agree with the expected values for all the tested materials.

Figure 3 shows the engineering stress–strain curves obtained from smooth and notched tensile samples in the as-received conditions, without hydrogenation.

As expected, the mechanical behavior of the tested steels is rather different. Hot-stamping and martensitic

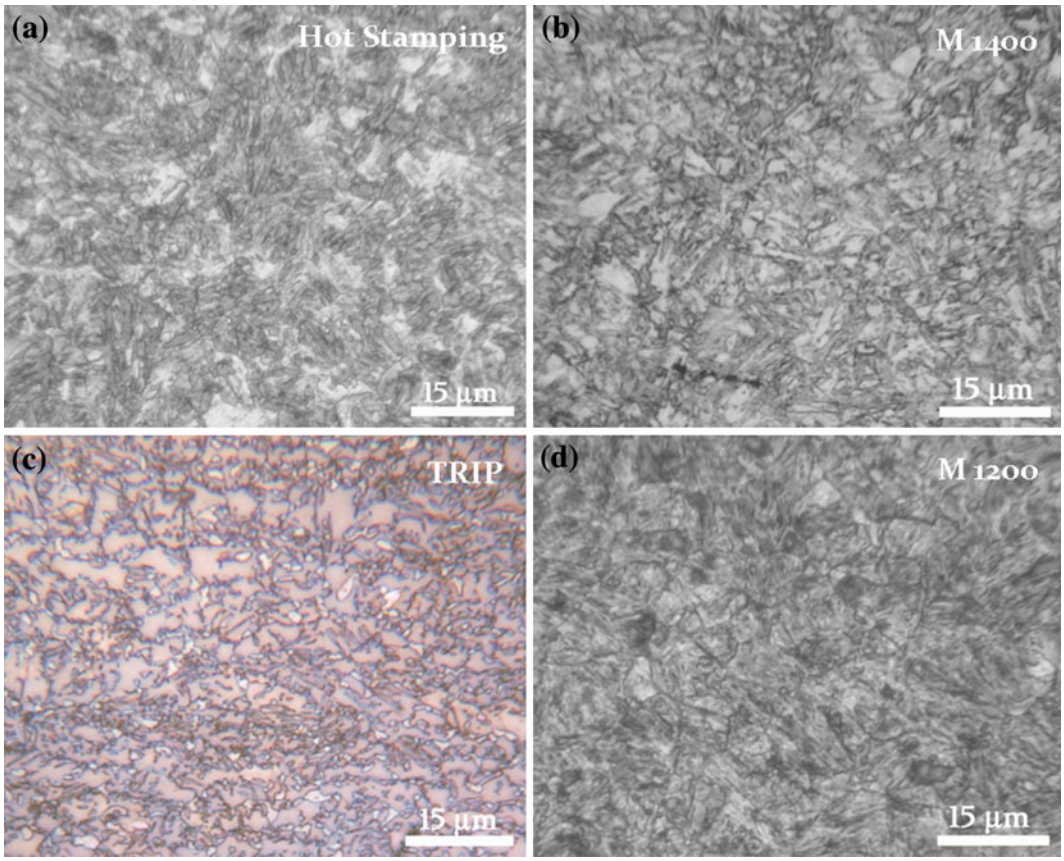

Fig. 2—Microstructures of tested advanced high strength steels. (*a*) Hot-stamping steel (nital reagent); (*b*) M 1400 steel (nital reagent); (*c*) TRIP 800 steel (Le Pera etchant): ferrite in light brown, bainite in dark brown, and martensite and austenite in white; and (*d*) M 1200 steel (nital reagent).

Table III. Mechanical Properties of the Analyzed Steels in the As-Received Conditions

	UTS (MPa)	YS (MPa)	Elongation (pct)
HS 1500	1615	1550	6
M 1400	1520	1410	5
M 1200	1305	1205	9
TRIP 800	815	620	26

YS: yield strength.

steels, which have a martensitic microstructure, show higher mechanical strength and lower ductility. On the contrary, TRIP 800 steel, characterized by a large strain-hardening effect associated with the presence of austenite in its microstructure, has very high ductility and lower strength.

C. *SSRT*

Figure 4 shows the engineering stress–strain curves obtained for notched samples when charged with different hydrogen contents. The reported hydrogen concentrations are the average values between the witness samples (hydrogenated together with tensile samples) representative of the pretensile hydrogen concentration and the post-tensile samples measured by using a region close to the fracture surface. Since samples are notched, the total elongation is short and thus so is the total time of the SSRT test. Thus, the measured differences between pretensile and post-tensile tests have been always less than 10 pct. Only three curves for each steel are shown in Figure 4: one relative to the as-received (without hydrogen) sample, one for the sample with the maximum tested hydrogen concentration, and another one for a medium level.

It can be easily observed that the hydrogen concentration ranges are different for different steels. This is because of the different hydrogen solubility in them and their uptake abilities, which are strictly dependent on the microstructure and the electrochemical properties of each steel.

In stress–strain diagram, hydrogen acts by reducing the extension of curve, without any (or with very poor) modification before the necking point. In the international scientific literature, different sensitive parameters are used as an indicator of hydrogen effect on steels, such as the fracture stress or the ductility (elongation or area) reduction.[10,14,22,23] This last parameter is better in the case of ductile and low work-hardening steels, where the fracture stress does not sensitively change with hydrogen content changes. On the contrary, for ultra high-strength steels, the elongation to fracture is not a

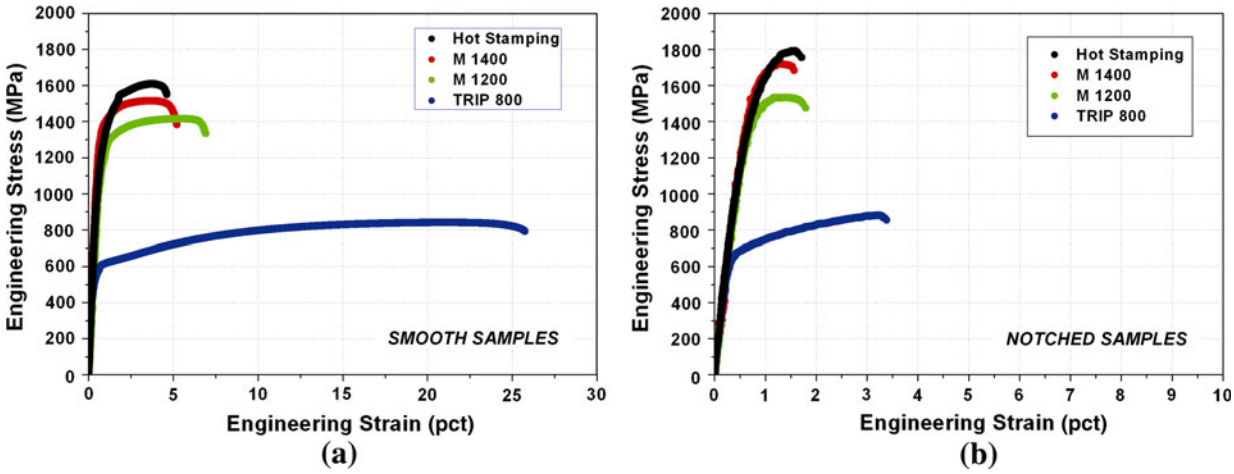

Fig. 3—Engineering stress–strain curves for the tested AHSS in the as-received (hydrogen uncharged) conditions. (*a*) Stress–strain curve for smooth samples. (*b*) Stress–strain curve for notched samples.

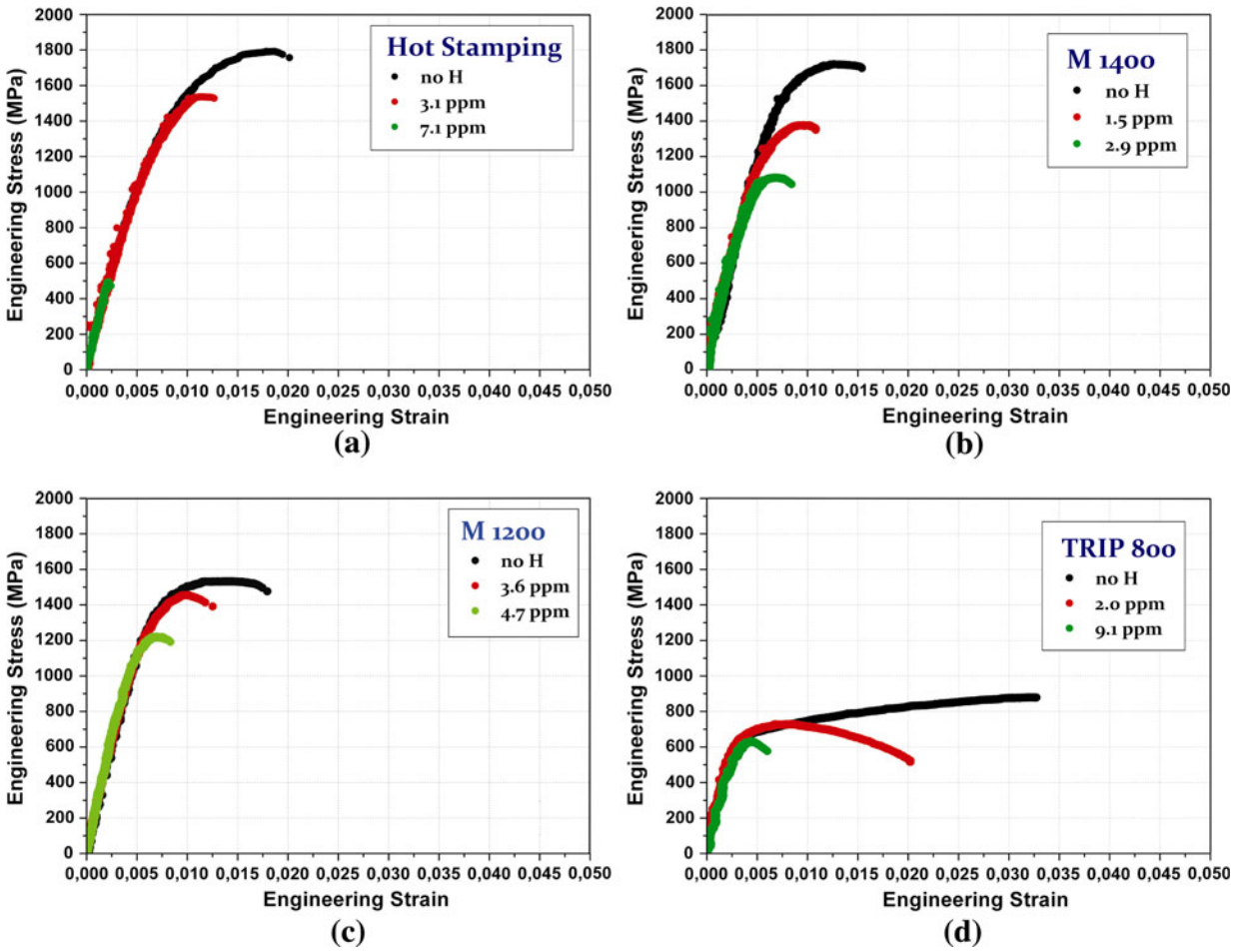

Fig. 4—Stress–strain curves of tested steels electrochemically charged at different hydrogen contents: (*a*) hot-stamping steel, (*b*) M 1400 steel, (*c*) M 1200 steel, and (*d*) TRIP 800 steel.

useful parameter because the hydrogen can induce a fracture in the elastic range, where the elongation of samples with different hydrogen content tends to show very similar values. Moreover, the presence of notch in tensile specimen further decreases the elongation to fracture sensitivity to hydrogen embrittlement (HE). Thus, the authors preferred to limit the analysis to fracture stress parameter.

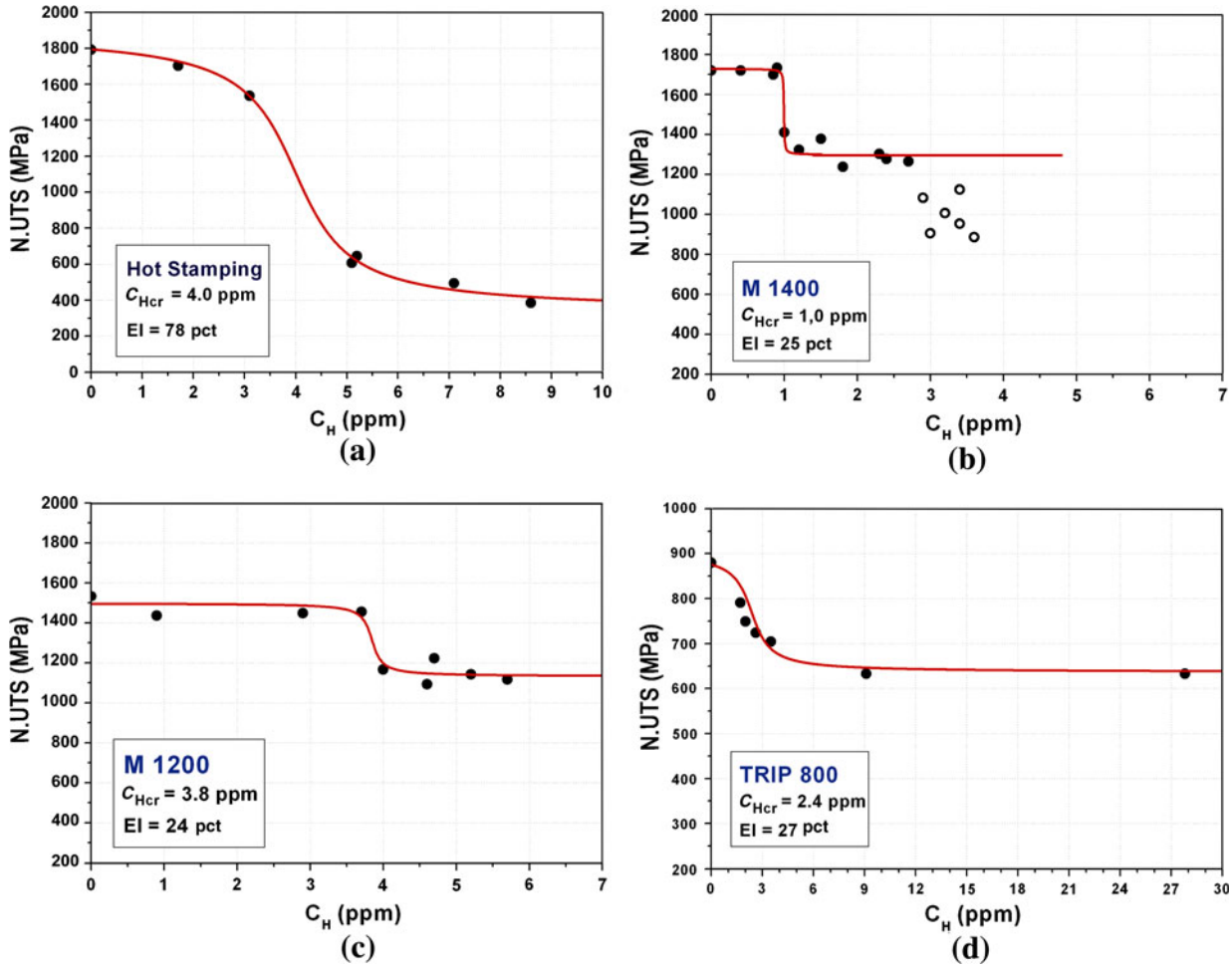

Fig. 5—Hydrogen embrittlement curves of tested steels: (*a*) hot-stamping steel, (*b*) M 1400 steel, (*c*) M 1200 steel, and (*d*) TRIP 800 steel. For each steel, the hydrogen critical concentration for embrittlement and the embrittlement index are reported. Some of the M1400 steel data are shown as hollow point in order to differentiate them in respect to the others. The meaning of this difference is described in text (detailed in Section IV–B). *N*.UTS is the UTS measured for notched specimen.

Figure 5 shows the so-called embrittlement curve of each steel, *i.e.*, the strength *vs* hydrogen concentration data. Strength values pass from values close to the as-received steel strength (for low hydrogen concentrations) to a lower plateau at higher hydrogen concentrations. These two plateaus are separated by a marked transition region. It is worth noting that this behavior is common for all the steel grades, from ductile to high-strength steels.[22,24,25] In order to interpolate the experimental data the following expression was used[22]:

$$N.\mathrm{UTS} = a - b \cdot \arctan\frac{C_\mathrm{H} - c}{d}$$

where *N*.UTS is the UTS of notched specimen; C_H is the hydrogen concentration; and *a*,*b*,*c*, and *d* are fitting parameters. In particular, the *c* parameter is related to the position of the inflection point (the middle of the transition region), *d* to the transition width, and *a* and *b* parameters to the plateau values.

As shown in Figure 5, the use of the "arctangent" function reproduces the experimental data well.

In order to identify the concentration at which value of the steel is affected by hydrogen embrittlement, the *c* value has been chosen as hydrogen critical concentration C_Hcr.

In Figure 5, the hydrogen critical concentration values C_Hcr related to each steel are reported, along with the embrittlement index (EI) calculated as follows:

$$\mathrm{EI} = \frac{N.\mathrm{UTS}_\mathrm{noH} - N.\mathrm{UTS}_\mathrm{max\,H}}{N.\mathrm{UTS}_\mathrm{noH}} \times 100$$

where $N.\mathrm{UTS}_\mathrm{noH}$ and $N.\mathrm{UTS}_\mathrm{maxH}$ are the UTS of notched specimens values of the uncharged sample and correspond with the maximum tested hydrogen concentration, respectively.

The embrittlement index is the percentage of *N*.UTS reduction measured at high hydrogen content in the concentration range correspondent to the low strength plateau. It is an indication of the maximum hydrogen effect on steel strength.

Results reported in Figure 5 show that the maximum EI value is reached for the hot-stamping steel (about 75 pct), whereas lower EI values (about 25 pct) are measured for the other ones.

Concerning the hydrogen critical concentration for embrittlement, the lowest value was found for M

1400 steel (about 1 wppm), while the other steels show higher values. The critical hydrogen concentration of TRIP 800 steel is about 2.5 wppm, and it is about 4 wppm for M 1200 and hot-stamping steels.

The embrittlement curve for M 1400 steel exhibits a further reduction of *N*.UTS after the low-strength plateau. This particular feature, related to a change in hydrogen damage modality, will be deeply discussed in Section IV.

D. *Hydrogen Absorbed During Painting Process*

Figure 6 shows the hydrogen concentration values measured from samples subjected to the real painting pretreatment. The reported measurement values are the average values calculated from three different samples.

All samples show an absorbed hydrogen concentration lower than about 0.4 wppm. As clearly visible in Figure 6, collected data do not show any specific trend related to the coating layer wholeness or to the painting cycle step.

IV. DISCUSSION

In Table IV, the main data extracted from SSRT tests are summarized.

It is worth noting that using very similar electrochemical charging conditions, the hydrogen concentration is very different from steel to steel. This feature mainly depends on different microstructural features. Also, martensitic steels with similar strength (HS1500 and M1400) showed very different hydrogen uptake ability. This is probably due to their different production process. HS 1500 is produced by the hot-rolling process, while M1400 steel is produced by the cold-rolling

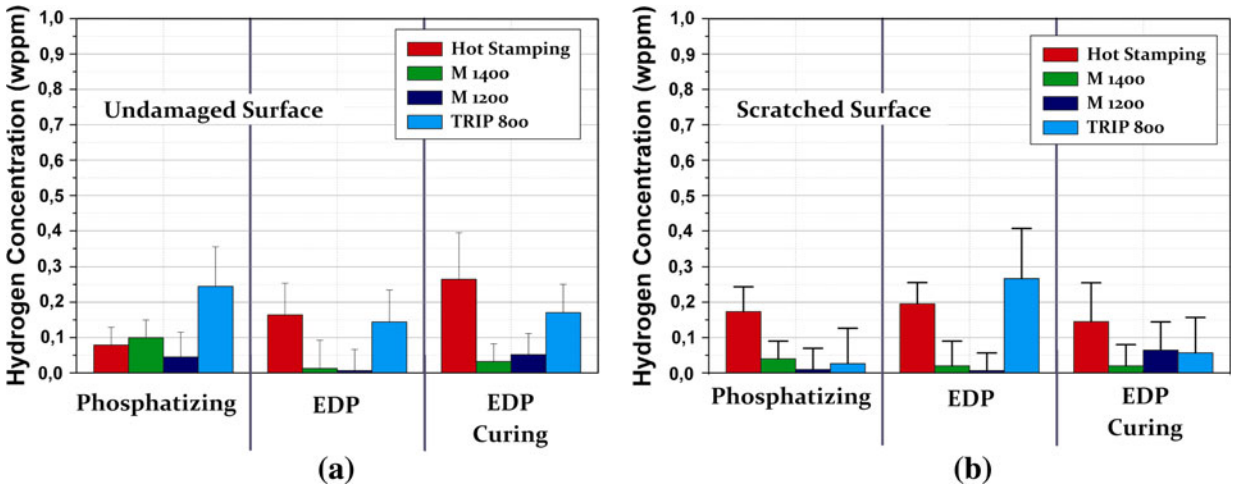

Fig. 6—Hydrogen concentration, measured by the electrochemical Barnacle method, absorbed during the following painting line steps: phosphatizing, electrodeposition painting, and final curing. (*a*) Results for undamaged surface and (*b*) results for scratched surface.

Table IV. Hydrogen Concentrations and Tensile Properties Measured in Function of Electrochemical Charging for all the Tested Steels

		Charging Conditions		
Steels	Parameters	Low*	High†	Very High‡
HS 1500	C (ppm)	1.8 ÷ 5.2	5.1 ÷ 8.6	
	N.UTS Red.§ (pct)	5 ÷ 65	65 ÷ 78	
	El. Red.‖ (pct)	10 ÷ 55	75 ÷ 90	
M 1400	C (ppm)	0.4 ÷ 1.8	1.5 ÷ 3.3	2.5 ÷ 3.6
	N.UTS Red.§ (pct)	0 ÷ 25	20 ÷ 42	25 ÷ 48
	El. Red.‖ (pct)	10 ÷ 15	35 ÷ 50	35 ÷ 60
M 1200	C (ppm)	0.9 ÷ 4.7	4.0 ÷ 5.8	
	N.UTS Red.§ (pct)	5 ÷ 28	23 ÷ 25	
	El. Red.‖ (pct)	0 ÷ 55	35 ÷ 65	
TRIP 800	C (ppm)	1.7 ÷ 3.5	2.6 ÷ 27.8	
	N.UTS Red.§ (pct)	10 ÷ 20	17 ÷ 27	
	El. Red.‖ (pct)	0 ÷ 75	40 ÷ 85	

*(Low): NaOH 0.1 N + As_2O_3 25 mg/L with current density between 1 and 10 mA/cm^2.
†(High): H_2SO_4 0.1 N + As_2O_3 25 mg/L with current density between 1 and 50 mA/cm^2.
‡(Very high): H_2SO_4 1 N + $NaAsO_2$ $5{\cdot}10^{-4}$ N with current density between 10 and 50 mA/cm^2.
§*N*.UTS Red. = Reduction of notched ultimate tensile strength in respect to uncharged sample.
‖El. Red. = Reduction of elongation to fracture in respect to uncharged sample.

process. Similar martensitic microstructure, little differences on its fineness, hardening, or chemical composition can induce heavy differences in hydrogen uptake ability. This is confirmed by all the performed tests, both for the electrochemical charging of SSRT specimens and for the hydrogen absorbed during painting, where HS 1500 steel showed final hydrogen concentration values much higher than M1400 and M1200 steels. Obviously, the presence of austenite phase in TRIP steel makes difficult the comparison with other steels in terms of hydrogen diffusivity and solubility. These differences induce also high differences in the hydrogen concentration range where the decreasing of mechanical properties appears, as visible in Figure 5.

In order to highlight the main hydrogen embrittlement properties, the results of each tested steel will be discussed in the following.

A. *Hot-Stamping Steel*

Although all steel grades can suffer hydrogen embrittlement,[9] high-strength steels are usually more prone to this problem. As expected, hot-stamping steel, characterized by a completely martensitic microstructure and very high strength levels (*N*.UTS of about 1600 MPa), shows a very high embrittlement index. The degradation of mechanical properties is very marked; for example, the strength of notched specimen with a hydrogen concentration of about 9 wppm is about 400 MPa, with a strength reduction of more than 75 pct.

The strength reduction of hot-stamping steels similar to that presented in this article has been reported in the literature.[11,14] Lee *et al*.[11] reported UTS values of about 400 MPa for samples charged to 1.7 wppm. The discrepancy in hydrogen content that has caused a similar EI in the Lee *et al*. work and the present data can be explained considering the difference in electrochemical charging conditions. They charged 1.7 mm in thickness tensile samples for only 30 minutes, but this time, according to the hydrogen diffusion coefficient (*D*) value, is not enough to produce a homogeneous hydrogen concentration inside the samples. Thus, close to the steel surface the hydrogen concentration could be much higher than in the center part. In the present work, *D* was calculated by using a Devanathan-Stackurski[18] electrochemical permeation apparatus, following the ASTM standard G 148-97.[26] Its value was about 6×10^{-7} cm^2/s. Using similar *D* values, for a 1.7 mm in thickness sample, a time of about 6 hours had been needed to reach uniform concentration across the specimen.[17] Finally, the low toughness of a completely martensitic steel causes the rupture of samples at the onset of subsurperficial cracks, even if the bulk material does have a hydrogen concentration much lower than the superficial one.

As shown in Figure 7(a), the fractographic analysis showed ductile fracture for the as-received sample. Increasing the hydrogen content, a typical hydrogen induced quasi-cleavage fracture appears (Figure 7(b)) with the presence of some fine secondary cracks. At a hydrogen concentration higher than the critical one, the secondary cracks enlarge and some intergranular component of primary crack can be highlighted, as visible in Figure 7(c).

Post-tensile samples have been sectioned in order to highlight the microstructural characteristic of the crack-initiation sites. Figure 8 shows some of these characteristics on the hot-stamping steel sample charged with 5.2 wppm of hydrogen. Both transgranular and intergranular fractures have been found as shown in Figures 8(a) and (b), respectively. The analysis has not shown any particular correlation between the crack onset and the microstructural features of HS steel.

B. *Martensitic Steels*

The embrittlement curve of M 1400 steel shows a critical concentration of about 1 wppm and an embrittlement index of about 25 pct.

In order to highlight the main factor influencing the hydrogen embrittlement susceptibility of martensitic steels, a deep microstructural analysis has been performed on longitudinal section of post-tensile samples in regions close to the failure surface. A great part of hydrogen cracks has been found to start from inclusion particles. The micrograph in Figure 9 shows a typical hydrogen crack generated on an inclusion particle for a sample of M 1400 steel charged at 3.0 wppm of hydrogen. The dangerous shape factor of elongated inclusions can contribute to an increase in the hydrogen embrittlement susceptibility.

Performing energy-dispersive X-ray spectroscopy microanalysis on inclusions, they have resulted to be constituted mainly by Ca, Si, Al, and Ti particles.

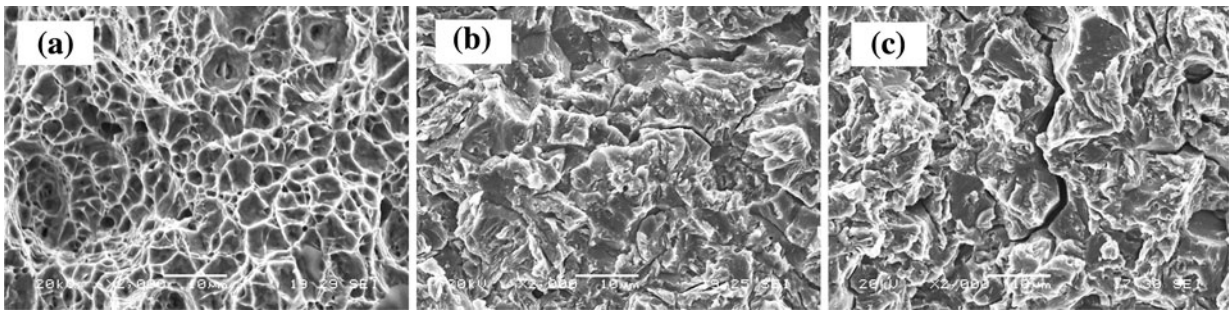

Fig. 7—Micrographs of fracture surface of hot-stamping steel samples charged with different hydrogen contents. (*a*) Uncharged specimen, (*b*) sample electrochemically charged at 2.6 wppm, and (*c*) sample electrochemically charged at 7.1 wppm.

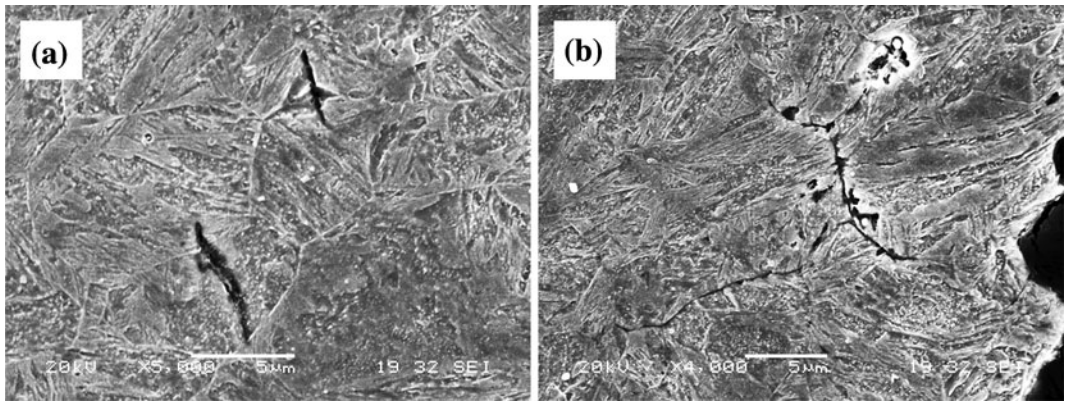

Fig. 8—Micrographs showing the longitudinal section of post-tensile hot-stamping steel sample (with 5.2 wppm) in the region close to the fracture surface. (*a*) Transgranular cracks and (*b*) intergranular cracks.

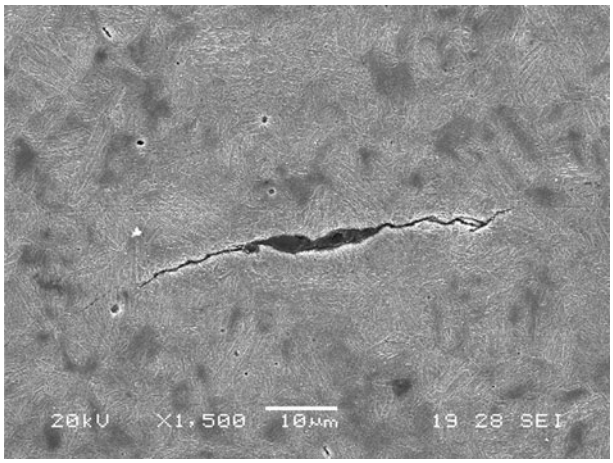

Fig. 9—Example of hydrogen-induced crack started from an inclusion particle, in a M 1400 steel electrochemically charged at 2.7 wppm.

Figure 10 shows the fracture surface for M 1400 samples with different hydrogen contents. The uncharged sample (Figure 10(a)) presents a ductile fracture, while hydrogenated samples are subjected to brittle fracture. For hydrogen concentration lower than about 2 wppm, samples have shown a mixed transgranular–intergranular fracture (Figure 10(b) for a 1.2 wppm charged sample), while for higher hydrogen content, there has been a predominance of intergranular fracture, as shown in Figure 10(c) for a sample charged at 3.0 wppm, as expected for the increasing of hydrogen activity.[27]

After the high concentration plateau, a further decrease of the strength level is clearly visible for M1400 steel, showed in Figure 5(b) as hollow points. Post-tensile fractographic analysis (Figure 11) showed that at a hydrogen concentration higher than about 3 wppm, the fracture surface changes appearance.

For lower hydrogen concentration, the low magnification fracture appearance is that typical of notched samples with a triangular area close to the notch associated with the stress intensification region (Figures 11(a) through (c)). For higher concentration, this morphology has disappeared and the fracture surface is composed of several elliptical cracks (Figure 11(d)). Deep secondary cracks are also clearly visible. This behavior has been probably due to the formation of hydrogen-induced cracks during the electrochemical charging, which greatly lower the sample strength. The failure of a sample with a concentration of about 4 wppm during electrochemical charging confirms the abovementioned explanation. The hydrogen induced cracks formed during electrochemical charging obviously have not the same extension and morphology in different samples. Thus the fracture stress measured in tensile test, heavely influenced by the presence of hydrogen induced cracks, have resulted very scattered. The authors have decided to not include these data in the embrittlement curve fitting, since this curve is valid for stress-assisted hydrogen embrittlement.

In the present explored experimental conditions, the hydrogen-induced cracks generated during electrochemical charging have been found only for the M 1400 steels, although the authors cannot exclude the possibility to induce hydrogen cracking on other steels at much higher hydrogen concentrations.

M 1200 steel shows an embrittlement curve similar to M 1400 steel. The lower strength level determines a lower hydrogen embrittlement susceptibility, shifting the hydrogen critical concentration to higher values (about 4 wppm).

Concerning the general hydrogen embrittlement behavior of very high-strength steels (with strength level higher than 1200 MPa) could be important to highlight the role of stamping modalities.

The hydrogen embrittlement susceptibility of high-grade martensitic steels could be increased by the fact that auto body components are produced by the cold stamping process that gives high residual stresses due to the springback effect.[28] Although the hot-stamping steel (comparable in terms of strength and ductility) has a much higher embrittlement index, the almost completely absent of residual stresses derived by the hot-stamping process can play favorably on its hydrogen embrittlement susceptibility.

C. *TRIP Steel*

The presence of austenite deeply influences the hydrogen behavior in steel. Thanks to the very high solubility

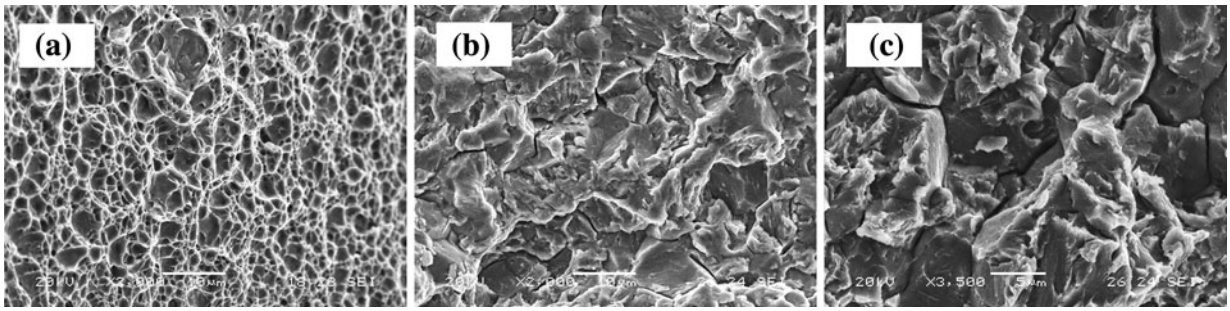

Fig. 10—Micrographs of fracture surface of M 1400 steel samples charged with different hydrogen contents. (*a*) Uncharged specimen, (*b*) sample electrochemically charged at 1.2 wppm, and (*c*) sample electrochemically charged at 2.7 wppm.

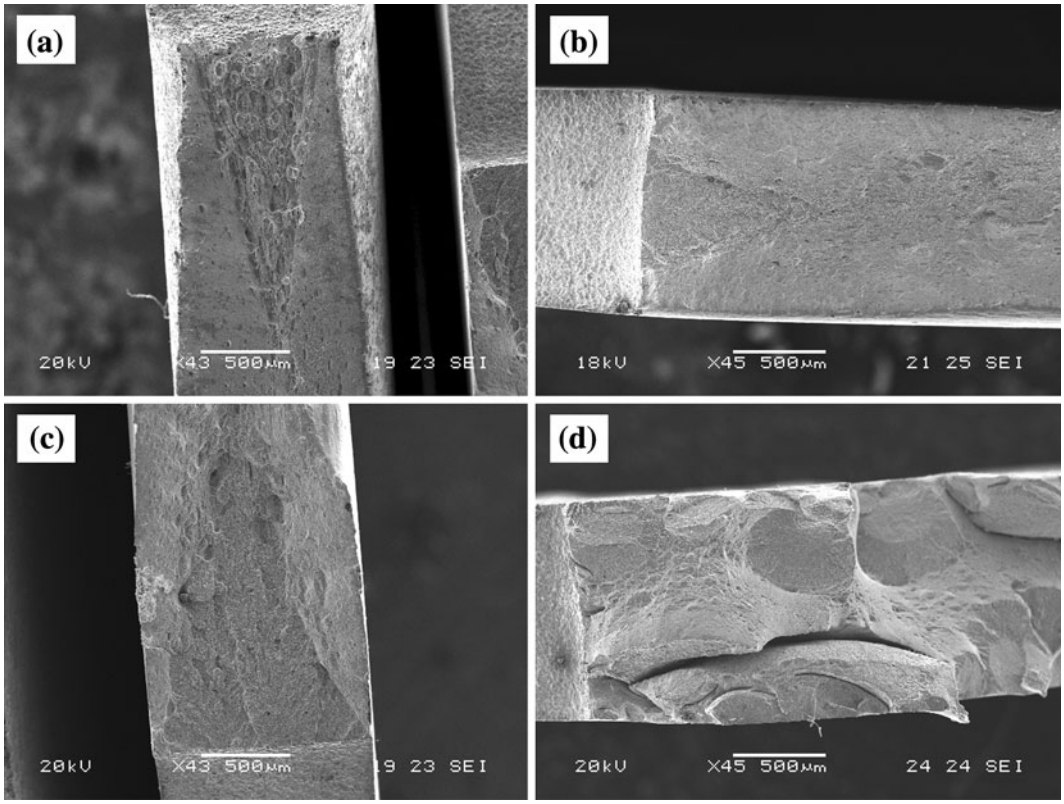

Fig. 11—SEM micrographs showing the fracture surface of M 1400 post-tensile samples with different hydrogen contents. (*a*) Uncharged specimen, (*b*) 0.9 wppm, (*c*) 2.3 wppm, and (*d*) 3.4 wppm.

and low diffusivity of hydrogen in it, austenite acts as a sink for hydrogen, lowering its mobility and increasing the final hydrogen concentration. Thus, in TRIP steel, the hydrogen concentration in austenite is much higher than in the other phase.

During the deformation of TRIP steels, austenite transforms into martensite (TRIP effect), which is the microstructure most susceptible to hydrogen embrittlement. Thus, it is fair to say that just after the application of stress, the hydrogen-enriched transformed martensite quickly cracks, inducing the failure of the specimen. Moreover, the not stable austenite of TRIP steels could be more and more unstabilized by the presence of hydrogen, as happens for austenitic stainless steels where hydrogen can induce martensitic transformation and related failure (for example, see Reference 29). Probably, this occurs because the embrittlement curve of TRIP 800 steel does not present a marked plateau in the low concentration region, as is clearly visible in Figure 5.

The microstructural examination of post-tensile samples electrochemically charged with hydrogen has shown the presence of crack onsets in correspondence of the hard particles, as shown for example in Figure 12. This result is in agreement with the above suggested fracture mechanism. Moreover, other research highlighted similar crack initiation mechanisms. Using EBSD techniques, Imlau *et al.*[26] found a high correlation between

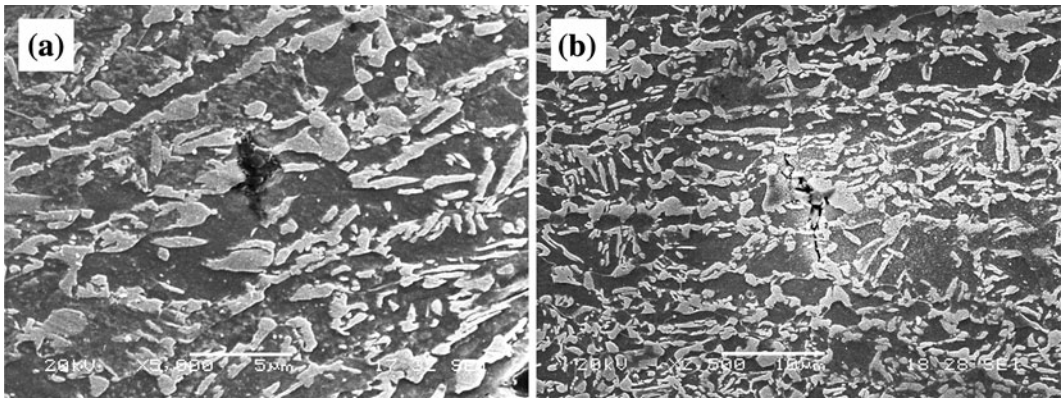

Fig. 12—Micrographs showing the longitudinal section of post-tensile TRIP 800 steel sample with different hydrogen contents in the region close to the fracture surface: (*a*) 3.5 wppm and (*b*) 28 wppm.

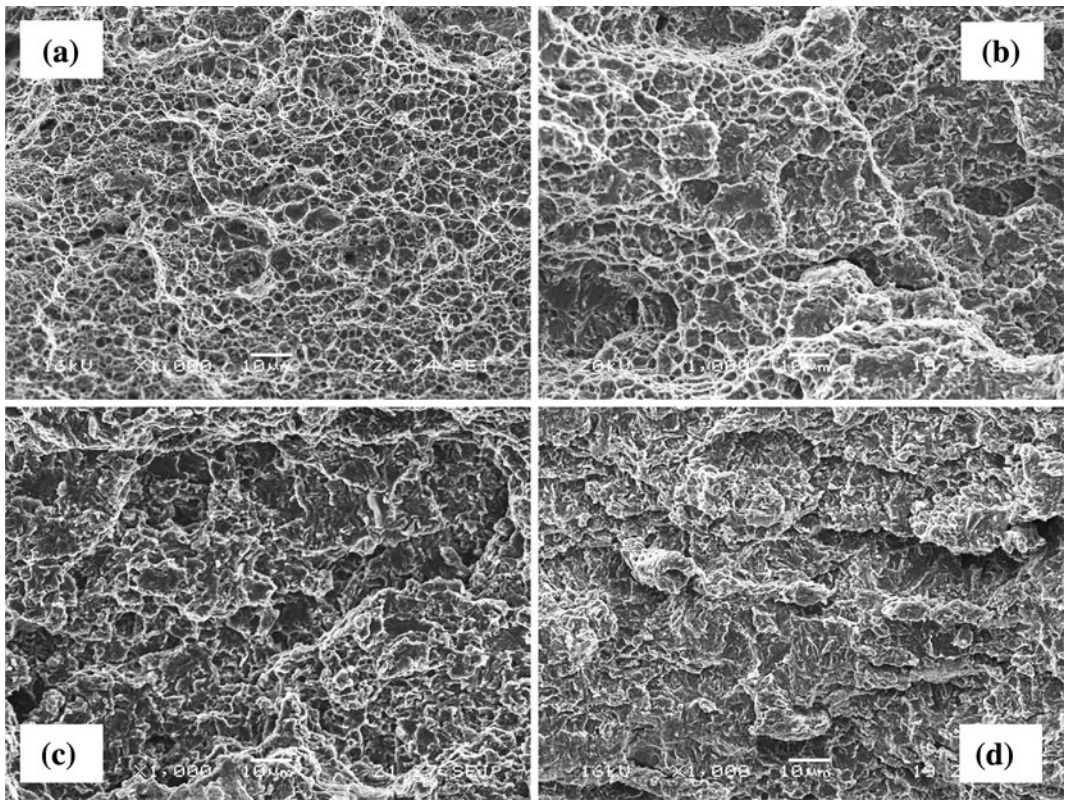

Fig. 13—Micrographs of fracture surface of TRIP 800 steel samples charged with different hydrogen contents. (*a*) Uncharged specimen, (*b*) sample electrochemically charged at 3.5 wppm, (*c*) sample electrochemically charged at 9.1 wppm, and (*d*) sample electrochemically charged at 28 wppm.

the region where cracks form and martensite transformation areas. Moreover, Ronevich *et al.*[14] found some cracks starting from hard particles (martensite islands) and propagating into ferrite grains.

Fractographic analysis has shown that fracture surfaces become more and more brittle by increasing the hydrogen content, as shown in Figure 13. The uncharged sample presents a completely ductile fracture (Figure 13(a)). After increasing the hydrogen content, the brittle percentage of fracture surface increases, above all for concentration higher than the critical one (Figure 13(b) through (d)).

Moreover, it is important to note that the ductile microstructure of TRIP 800 steel and the low tested grade (compared with the other tested steels) limit the strength reduction in presence of high hydrogen concentration to about 25 pct.

Despite the presence of austenitic phase that is usually considered to have higher hydrogen embrittlement resistance thanks to its higher toughness and its lower

hydrogen diffusivity, TRIP 800 steel shows some susceptibility to hydrogen embrittlement in respect to its low grade. The high hydrogen uptake ability due to austenite presence in microstructure, along with the tendency of this phase to transform into an embrittled martensitic phase, make this class of steel suscetible to hydrogen embrittlement, at least in case of high hydrogen external activity and stress level.

D. *Hydrogen Absorbed During Body in White Painting Process*

The hydrogen critical concentrations measured by SSRT tests are not an exhaustive expression of the hydrogen embrittlement susceptibility of a steel. This value has to be correlated to the hydrogen concentration absorbed in the real conditions during the production process or service life of the steel components.

The measurement of hydrogen content absorbed during the painting pretreatment processes of body in white has been performed in an industrial plant during a real treatment. In this way, the coupons of the analyzed steels have exactly followed the same process of real cars. As already detailed, two types of samples have been used, one with the coating layer undamaged and another one with scratches, in order to simulate damage on the coating layer.

As reported in Figure 6, the measured hydrogen contents have been always less than 0.4 wppm in all the tested conditions (after phosphatizing, after EDP, and after EDP curing line steps). This means that for all the tested steels, the absorbed hydrogen is much lower than the hydrogen critical concentration. Hot-stamping and TRIP 800 steels showed the highest values of absorbed hydrogen, while martensitic steels showed lower tendency to be hydrogenated. Concerning TRIP 800 steel, its hydrogen uptake ability was derived above all by the austenitic phase present in the microstructure.

The measured hydrogen concentrations show the same differences observed during electrochemical charging of tensile samples, being much higher for hot-stamping and TRIP 800 steels than martensitic steels, highlighting a different hydrogen uptake ability. No trend is visible either in function of the steel grade, or of the cycle steps.

Considering the highest hydrogen concentration measured for each steel and using the interpolation formula of the embrittlement curve, it is possible to calculate the strength of materials after the painting process. The strength reduction is less than 1 pct for all the tested steels. Thus, *de facto*, they do not suffer hydrogen embrittlement after the BIW production process.

Moreover, since BIW is mainly assembled using cold-formed components, some coupons of the analyzed steels have been bended up to reach the 80 pct of the ultimate real stress.

In order to analyze their hydrogen-delayed cracking susceptibility during painting, these coupons followed the same painting line as for the measurement of absorbed hydrogen. Then bended samples were taken into observation for two weeks in order to register the time to eventual cracks formation. The time of two weeks is greater than that needed to make the hydrogen concentration zero in the coupon (that, thanks to the short time of process, was able to absorb hydrogen only in the surface). No cracks have been found in all of the tested steels, thus confirming the absence of hydrogen embrittlement associated to the autobody production process. Nevertheless, further investigations will be performed in order to highlight the possible hydrogen uptake during the car service life.

V. CONCLUSIONS

From the above-mentioned tests performed on AHSS, it is possible to highlight the following conclusions:

1. Hot-stamping steel has shown a heavy reduction of tensile strength (more than 75 pct) for a hydrogen concentration of about 7 wppm. As expected, its fully martensitic microstructure is highly susceptible to hydrogen embrittlement.
2. Martensitic steels with a very high tensile strength have shown a hydrogen critical concentration of about 1 and 4 wppm for M 1400 and M 1200 steels, respectively. In the analysis of crack initiation sites, a predominance of hydrogen-induced defects in correspondence of inclusion particles has been found. These defects can contribute to the hydrogen embrittlement susceptibility of this steel class. Moreover, M 1400 steel has demonstrated a high hydrogen-induced cracking susceptibility at a hydrogen concentration higher than about 3 wppm, with the formation of cracks during the electrochemical charging. M 1200 steel, thanks to its lower resistance, has a higher hydrogen critical concentration, and it does not show a tendency to crack in the absence of external stresses.
3. Although the presence of the austenitic phase is in its microstructure, the analyzed TRIP 800 steel has shown some susceptibility to hydrogen embrittlement. Its hydrogen critical concentration is about 2,5 wppm. This behavior has been correlated to the presence of austenite that transforms into martensite during deformation. The high hydrogen solubility in this phase can increase the tendency to transform and can produce a hydrogen-rich martensitic phase that quickly cracks during straining.
4. The hydrogen concentration absorbed during the pretreatment of the painting cycle has shown values much lower than the critical concentrations in all the analyzed conditions. Moreover, no hydrogen-induced delayed cracks have been found on the bended region of the same samples. These results suggest that the tested AHSS can be used to build BIW components with a good safety factor.

REFERENCES

1. International Iron & Steel Institute Committee on Automotive: Advanced High Strength Steel (AHSS) Application Guidelines, Version 3, 2006, www.worldautosteel.org.
2. C. Federici, S. Maggi, and S. Rigoni: *Proc. Conf. on New Developments on Metallurgy and Applications of High Strength Steels*, Buenos Aires, Argentina, 2008.
3. Y. Mukai: *Kobelco Tech. Rev.*, 2005, no. 26, pp. 26–31.
4. B.C. De Cooman, L. Chen, H.S. Kim, Y. Estrin, S.K. Kim, and H. Voswinckel: *Proc. Conf. on New Developments on Metallurgy and*

Applications of High Strength Steels, Buenos Aires, Argentina, 2008.
5. W. Bleck and K. Phiu-On: *Mater. Sci. Forum*, 2005, vol. 500/501, pp. 97–114.
6. R.A. Oriani, J.P. Hirth, and M. Smialowski: *Hydrogen Degradation of Ferrous Alloys*, Noyes Publications, Park Ridge, NJ, 1985.
7. J.P. Hirth: *Metall. Trans. A*, 1980, vol. 11A, pp. 861–90.
8. *ASM Materials Handbook: Metals Handbook*, 9*th* ed., vol. 13, ASM International, Materials Park, OH, 1987, p. 330.
9. I.M. Bernstein: *Proc. 5th Int. Conf. on the Effect of Hydrogen on the Behavior of Materials*, A.W. Thompson and N.R. Moody, eds., TMS, Warrendale, PA, 1996, pp. 3–11.
10. T.B. Hilditch, S-B. Lee, J.G. Speer, and D.K. Matlock: *SAE SP*, 2003, vol. 1764, pp. 47–56.
11. S-J. Lee, J.A. Ronevich, G. Krauss, and D. Matlock: *ISIJ Int.*, 2010, vol. 50 (2), pp. 294–301.
12. K.H. So, J.S. Kim, Y.S. Chun, K.T. Park, Y-K. Lee, and C.S. Lee: *ISIJ Int.*, 2009, vol. 49 (12), pp. 1952–1959.
13. H. Mohrbacher: *Proc. Conf. on Steel Product Metallurgy and Application*, Pittsburgh, PA, 2008.
14. J.A. Ronevich, J.G. Speer, and D.K. Matlock: *SAE Int. J. Mater. Manuf.*, 2010, vol. 3 (1), pp. 255–67.
15. W.J. Pollock: *ASTM-STP 962, Hydrogen Embrittlement: Prevention and Control*, L. Raymond, ed., ASTM STP 962, Philadelphia, PA, 1988, pp. 68–80.
16. I. Krylova: *Progr. Org. Coating.*, 2001, vol. 42, pp. 119–31.
17. J. Cranck: *The Mathematics of Diffusion*, 2nd ed., Oxford Science Publications, Oxford, U.K., 1975, pp. 49–51.
18. M.A.V. Devanathan and Z. Stachurski: *Proc. R. Soc. London, Ser. A*, 1962, vol. 270, no. 1340, pp. 90–102.
19. ASTM G129 – 00 (reapproved 2006): *Standard Practice for Slow Strain Rate Testing to Evaluate the Susceptibility of Metallic Materials to Environmentally Assisted Cracking*, ASTM International, West Conshohoken, PA, 2006.
20. D.A. Berman and V.S. Agarwala: *ASTM-STP 962 Hydrogen Embrittlement: Prevention and Control*, L. Raymond, ed., ASTM STP 962 Philadelphia, PA, 1988, pp. 98–104.
21. ASTM F 1113 – 87 (reapproved 2005): *Standard Test Method for Electrochemical Measurement of Diffusible Hydrogen in Steels (Barnacle Electrode)*, ASTM International, West Conshohoken, PA, 2005.
22. M. Beghini, G. Benamati, L. Bertini, I. Ricapito, and R. Valentini: *J. Nucl. Mater.*, 2001, vol. 288, pp. 1–6.
23. E. Akiyama, S. Li, Z. Zhang, M. Wang, K. Matsukado, K. Tsuzaki, and B. Zhang: *Proc. 2008 Int. Hydrogen Conf.*, B. Somerday, P. Sofronis, and R. Jones, eds., ASM International Materials Park, OH, 2009, p. 54–61.
24. R. Valentini, A. Solina, S. Matera, and P. De Gregorio: *Metall. Mater. Trans. A*, 1996, vol. 27A, pp. 3773–80.
25. G. Lovicu, M. De Sanctis, A. Dimatteo, R. Valentini, and P. Trombetti: 32° *Convegno Nazionale AIM*, Ferrara, Italy, 2008.
26. ASTM G148-97 (reapproved 2003), *Standard Practice for Evaluation of Hydrogen Uptake, Permeation, and Transport in Metals by an Electrochemical Technique*, 2003.
27. C.J. McMahon, X. Liu, J. Kameda, and M.J. Morgan: *Proc. 2008 Int. Hydrogen Conf.*, B. Somerday, P. Sofronis, and R. Jones, eds., ASM International, Materials Park, OH, 2009, pp. 46–53.
28. *Die Design Handbook*, Society of Manufacturing Engineers (SME), Dearborn MI, 1990, pp. 6–9.
29. S.M. Teus, V.N. Shyvanyuk, and V.G. Gavriljuk: *Mater. Sci. Eng. A*, 2008, vol. 497, pp. 290–94.